Systematic description of evaporation spectra for light and heavy compound nuclei

R. J. Charity
Department of Chemistry, Washington University, St. Louis, Missouri 63130, USA
(Received 7 May 2010; published 14 July 2010)

To systematically describe evaporation spectra for light and heavy compound nuclei over a large range of excitation energies, it was necessary to consider three ingredients in the statistical model. First, transmission coefficients or barrier penetration factors for charged-particle emission are typically taken from global fits to elastic-scattering data. However, such transmission coefficients do not reproduce the barrier region of evaporation spectra and reproduction of the data requires a distributions of Coulomb barriers. This is possibly associated with large fluctuations in the compound-nucleus shape or density profile. Second, for heavy nuclei, an excitation-energy dependent level-density parameter is required to describe the slope of the exponential tails of these spectra. The level-density parameter was reduced at larger temperatures, consistent with the expected fadeout of long-range correlation, but the strong A dependence of this effect is unexpected. Last, to describe the angular-momentum dependence of the level density in light nuclei at large spins, the macroscopic rotational energy of the nucleus has to be reduced from the values predicted with the finite-range liquid-drop model.

DOI: 10.1103/PhysRevC.82.014610 PACS number(s): 21.10.Ma, 24.60.Dr, 25.70.Jj

I. INTRODUCTION

The statistical model of compound-nucleus (CN) decay is extensively used in pure and applied nuclear science. In many reaction scenarios one or more compound nuclei are formed after a nuclear collision. Compound nuclei are equilibrated in their nondecay degrees of freedom and thus their decay is independent of how they were created. Statistical-model codes have been used as "afterburners" in many reaction-modeling programs decaying the simulated compound nuclei produced from some initial fast-reaction mechanism. The initial reaction could be fusion, spallation, fragmentation, etc.

Accurate determination of the statistical-model parameters at high excitation energies would give insight into the properties of hot nuclei. The level densities are sensitive to the magnitude of long-range correlations associated with collective excitations, transmission coefficients are sensitive to the charge and mass distributions, and fission maybe sensitive to the nuclear viscosity. Efforts to extract such information require systematic studies of CN decay covering a large range of CN Z,A and excitation energy.

The modeling of spallation reactions is important in applications ranging from transmutation of nuclear waste, the design of neutron sources for condensed-mater studies, radiation protection around accelerators and in space, and the production of rare isotopes for nuclear and astrophysics experiments. The modeling of such reactions involves an intranuclear cascade [1,2] or quantum molecular dynamics code [3] to simulate the production of the initial fast-reaction products and the properties of the residual compound nuclei formed (Z, A, E^*, and J joint distributions). These compound nuclei then deexcited with a statistical-model code, which includes evaporation and fission and possible other decay modes. The residual nuclei are predicted to be excited to large excitation energies (many hundreds of MeV) and therefore knowledge of the statistical-model parameters is needed for this energy regime.

The final predictions of spallation modeling are sensitive to both the statistical-model parameters and those associated with the initial fast phase of the reaction. When fitting experimental spallation data, it is not always possible to isolate the role of the statistical-model parameters and constrain them. Alternatively, heavy-ion-induced complete-fusion reactions can be used to create compound nuclei. In complete fusion, the excitation energy and identity of the CN are completely defined from conservation laws. The CN spin distribution can also be well constrained. The maximum spin can be determined from measurements of the total fusion cross section or, alternatively, simple one-dimensional models are generally quite accurate above the fusion barrier. Thus, the simple complete-fusion mechanism with no fast nonstatistical particles and a well-defined distribution of CN provides an opportunity to constrain the statistical-model parameters.

Of course, complete-fusion reactions are limited by pre-equilibrium emissions and incomplete-fusion processes, which sets it at large bombarding energies (>10 MeV/A). However, large excitation energies (up to $\sim$250 MeV) can still be probed with complete fusion using more symmetric reactions. Heavy-ion-induced fusion reactions, especially the more symmetric cases, emphasize large spins, typically larger than those probed by spallation reactions at the same excitation energies. Therefore, application of statistical-model parameters determined in fusion reactions to spallation modeling requires a good understanding of the spin dependence of CN decay.

The statistical model has a long history in heavy-ion-induced fusion reactions and has been fit to a large body of data, including fission probabilities, light-particle evaporation spectra, residual Z and A distributions, γ-ray multiplicities, etc. Although such data are usually fit within the statistical-mode framework, it has generally been found to be necessary to fine tune the statistical-model parameters for a particular CN or mass region. No statistical-model prescription exists that gives accurate predictions of these quantities over the entire table of isotopes. This work starts to address these problems by concentrating on light-particle evaporation, which is sensitive to the excitation energy and spin dependencies of the nuclear level density and the transmission coefficients for penetration of the Coulomb barriers hindering particle emission.

The assumption that the decay of the CN is independent of how it was created may not always be correct in fusion reactions. At high excitation energies when the statistical lifetime approaches the fusion time scales, dynamical effects may occur which depend on the entrance-channel mass asymmetry. Specifically symmetric reaction channels are predicted to dissipate the entrance-channel kinetic energy more slowly and may start particle evaporation before the fusion dynamics is complete. There have been many studies of entrance-channel dependence of CN decay. However, taken as a whole, no clear consistent picture has emerged from these studies and in a number of cases their conclusions are contradictory. In particular, concerning the shapes of evaporation spectra, one should note three studies where α-particle spectra were measured for different entrance channels, but with matched excitation-energy and spin distributions. Cinausero *et al.* found no entrance-channel dependence of the spectral shape for $A \sim 160$ compound nuclei at $E^* \sim 300$ MeV formed in ^{86}Kr + ^{76}Ge, ^{16}O + ^{150}Sm, and ^{60}Ni + ^{100}Mo reactions [4]. For $E^* = 170$ MeV ^{164}Yb compound nuclei formed in ^{16}O + ^{148}Sm and ^{64}Ni + ^{100}Mo reactions, Charity *et al.* noted a slight enhancement in the α-particle yield in the sub-barrier region; otherwise, the kinetic-energy spectra were consistent [5]. However, Liang *et al.* reported on entrance-channel dependencies of the slope of the high-energy tail in $E^* =$ 113-MeV ^{156}Er compound nuclei formed in ^{12}C + ^{144}Sm, ^{35}Cl + ^{121}Sb, and ^{60}Ni + ^{96}Mo reactions [6]. It is difficult to reconcile the three studies because they pertain to the same mass region. In this work we ignore such effects and assume that, if they exist, they are small at least compared to the overall variations owing to the mass, excitation-energy, and spin dependences of the statistical-model parameters

Statistical-model parameters are extracted from comparison of statistical-model calculations to experimental data. In this work, all statistical-model calculations were performed with the code GEMINI++ [7] written in the C++ language. This is a successor of the well known statistical-model code GEMINI [8] written in FORTRAN.

II. DATA

The data used in this work to constrain the statistical-model parameters come from many experimental studies covering a wide range of CN masses. The CN, the reactions, the excitation energies, and references are listed in Table I. For CN with $A > 150$, only studies where light particles were detected in coincidence with evaporation residues were used. For the lighter systems, only inclusive spectra are available. By appropriate selection of detection angle [backward (forward) angles for normal (reverse) kinematics reactions], one can isolate proton and α-particle spectra which are dominated by CN emission though some contamination from other reaction processes is possible for the lowest kinetic energies [9]. This is discussed in more detail in Sec. V.

While the residue-gated spectra may be cleaner, they may suffer from distortions owing to the limited kinematic acceptance of the residue detectors. For example, detection of evaporation residues at large angles enhances high-energy particles as these give the largest recoil kick to the residue, enabling it to get to such angles. The spectra used in this work were either corrected for this effect in referenced studies, or, for the ^{160}Yb CN, the GEMINI++ simulations were gated on the experimental residue acceptance.

It is important in the statistical-model calculations to have realistic spin distributions for the compound nuclei. The fusion cross section as a function of spin was assumed to have the form

$$\sigma_{\rm fus}(J) = \pi\lambda^2 \sum \frac{(2J+1)}{1+\exp\left(\frac{J-J_0}{\delta J}\right)}. \quad (1)$$

The quantity J_0 can be constrained from the fusion cross section. This is either measured, constrained from systematics, or obtained from the Bass model [10], which is reasonably accurate for the systems under study. The parameter δJ was varied from 2 to 10 $\hbar$ with increasing asymmetry of the entrance channel. However, in this work, the sensitivity of the predicted evaporated spectra to this parameter is very small.

Fission competition is also important for determining the J values that give rise to evaporation residues. When available (Table I), fission and/or evaporation-residue cross sections were fit by adjusting the fission parameter a_f/a_n of Sec. IV D. Otherwise, interpolated values of a_f/a_n were used. A more detailed discussion of the fission parameters in GEMINI++ can be found in Ref. [11].

III. EVAPORATION FORMALISM

Because GEMINI++ is to be used for CN with high spins, the evaporation of light particles is treated with the Hauser-Feshbach formalism [32], which explicitly takes into account the spin degrees of freedom. The partial decay width of a CN of excitation energy E^* and spin $J_{\rm CN}$ for the evaporation of particle i is

$$\Gamma_i(E^*, J_{\rm CN}) = \frac{1}{2\pi\rho_{\rm CN}(E^*, J_{\rm CN})} \int d\varepsilon \sum_{J_d=0}^{\infty} \sum_{J=|J_{\rm CN}-J_d|}^{J_{\rm CN}+J_d} \times \sum_{l=|J-S_i|}^{J+S_i} T_\ell(\varepsilon)\rho_d(E^* - B_i - \varepsilon, J_d), \quad (2)$$

where J_d is the spin of the daughter nucleus; S_i, J, and ℓ, are the spin, total, and orbital angular momenta of the evaporated particle; ε and B_i are is its kinetic and separation energies; T_ℓ is its transmission coefficient or barrier penetration factor; and ρ_d and $\rho_{\rm CN}$ are the level densities of the daughter and CN, respectively. The summations include all angular momentum couplings between the initial and final states. In GEMINI++, the Hauser-Feshbach formalism is implemented for the n, p, d, t, ^{3}He, α, ^{6}He, $^{6-8}$Li, and $^{7-10}$Be channels. However, in this work, we just compare predicted kinetic-energy spectra to experimental results for the p, α, and occasional n channels. GEMINI++ also allows for intermediate-mass fragment emission following the formalism of Moretto [33]. However, these decay modes are not very important for the calculations of this work.

The nuclear level density is often approximated by the Fermi-gas form [34] derived for a spherical nucleus in the independent-particle model with constant single-particle level

TABLE I. Experimental data used in this work indicating the compound nucleus (CN), the beam energy $E_{\rm beam}$, the excitation energy E^*, the fusion reaction, the evaporation spectra measured (n,p,α), and the values of J_0 defining the angular-momentum distribution of Eq. (1). The first listed references refer to the study that measured the kinetic energy spectra. The σ references refer to measurements of the fission and residues cross sections used to constrain J_0 and the fission probability.

CN	$E_{\rm beam}$ (MeV)	E^* (MeV)	Reaction	Ref.	Spectra	σ Refs.	J_0
^{59}Cu	100	58	^{32}S + ^{27}Al	[12]	α	[13–16]	27[a]
	105	60		[17]	α	[13–16]	30[a]
	130	72		[12]	α	[13–16]	34[a]
	140	77		[12]	α	[13–16]	38[a]
	150	82		[12]	α	[13–16]	39[a]
	214	110		[17]	α	[13–16]	45[a]
^{67}Ga	187	90	^{40}Ar + ^{27}Al	[18]	p,α		46[b]
	670	127	^{55}Mn + ^{12}C	[19]	p,α		42[b]
	280	127	^{40}Ar + ^{27}Al	[19]	p,α		54[b]
^{96}Ru	180	113	^{32}S + ^{64}Ni	[20]	p,α		69[b]
^{106}Cd	160	99	^{32}S + ^{74}Ge	[21]	p,α		68[c]
	99	291		[21]	p,α		83[c]
	99	291		[21]	p,α		89[c]
	99	291		[21]	p,α		89[c]
^{117}Te	81	71	^{14}N + ^{103}Rh	[22]	p,α		40[c]
	146	71	^{40}Ar + ^{77}Se	[23]	p,α		52[c]
	121	106	^{14}N + ^{103}Rh	[22]	p,α		53[c]
^{156}Er	142	113	^{12}C + ^{144}Sm	[6]	p,α	[6]	54[a]
	218	113	^{35}Cl + ^{121}Sb	[6]	p		>86[d]
	333	113	^{60}Ni + ^{96}Zr	[6]	p,α	[24]	>90[d]
^{160}Yb	300	91	^{60}Ni + ^{100}Mo	[25]	n,p,α	[25]	>90[d]
	360	129		[25]	n,p,α	[25]	>90[d]
	420	166		[25]	n,p,α	[25]	>90[d]
	480	204		[25]	n,p,α	[25]	>90[d]
	546	245		[25]	n,p,α	[25]	>90[d]
^{193}Tl	145	65	^{28}Si + ^{160}Ho	[26]	p,α	[26]	46[a]
	166	83		[26]	p,α	[26]	68[a]
	193	106		[26]	p,α	[26]	80[a]
	216	125		[26]	p,α	[26]	96[a]
^{200}Pb	121	86	^{19}F + ^{181}Ta	[27]	p,α	[27]	56[a]
	154	116		[27]	p,α	[27]	72[a]
	179	139		[27]	p,α	[27]	83[a]
	195	153		[27]	p,α	[27]	89[a]
^{224}Th	114	59	^{16}O + ^{208}Pb	[26]	p,α	[28–30]	51[a]
^{224}Th	138	82		[26]	p,α	[28–30]	67[a]

[a]The J_0 is constrained from the measured fusion cross section.
[b]The J_0 values were obtained from the referenced studied where the fusion cross section was estimated from the systematics of Ref. [31].
[c]The J_0 values were estimated from the Bass model [10].
[d]The J_0 values are large and the residue cross section is determined solely by fission competition. Fission parameters were adjusted to reproduce measured evaporation residues.

densities,

$$\rho_{\rm FG}(E^*, J) = \frac{(2J+1)}{24\sqrt{2}a^{1/4}U^{5/4}\sigma^3}\exp(S), \tag{3}$$

$$S = 2\sqrt{aU}, \tag{4}$$

where S is the nuclear entropy and the level-density parameter is

$$a = \frac{\pi^2}{6}\left[g^n\left(\varepsilon_F^n\right) + g^p\left(\varepsilon_F^p\right)\right]. \tag{5}$$

Here $g^n(\varepsilon_F^n)$ and $g^p(\varepsilon_F^p)$ are the neutron and proton single-particle level densities at their respective Fermi energies and

$$U = E^* - E_{\rm rot}(J), \quad E_{\rm rot} = \frac{J(J+1)\hbar^2}{2\mathcal{I}_{\rm rig}}, \tag{6}$$

$$\sigma^2 = \mathcal{I}_{\rm rig}T. \tag{7}$$

The quantity $\mathcal{I}_{\rm rig}$ is the moment of inertia of a rigid body with the same density distribution as the nucleus and T is the

nuclear temperature:

$$\frac{1}{T} = \frac{dS}{dU}. \tag{8}$$

The quantity U can be interpreted as a thermal excitation, after the rotational energy of the nucleus is removed.

At large angular momenta, macroscopic models of the nucleus such as the rotating liquid-drop model (RLDM) [35] and Sierk's Yukawa-plus-exponential finite-range calculations [36] predict that the nuclear shape distorts to accommodate the centrifugal forces. Many implementations of the statistical model, including GEMINI++, generalize Eq. (7) by the replacing $E_{\rm rot}(J)$, the rotational energy of a spherical nucleus of fixed moment of inertia, with $E_{\rm yrast}(J)$, the deformation-plus-rotational energy predicted by these macroscopic models where the deformation increased with spin. In GEMINI++, the Sierk predictions of $E_{\rm yrast}(J)$ are used for all but the lightest compound nuclei (see Sec. V).

The shape of the kinetic-energy spectra of an evaporated particle is thus sensitive to three ingredients:

(i) the magnitude of the level-density parameter and its excitation-energy dependence,
(ii) the transmission coefficients,
(iii) the angular-momentum dependence of $E_{\rm yrast}(J)$.

The level-density parameter defines the slope of the exponential tail of the evaporation spectrum while the transmission coefficients define the shape in the Coulomb barrier region and the effects of these two ingredients are easily isolated when comparing to data. The angular-momentum dependence of $E_{\rm yrast}(J)$ is most important in light nuclei where the moments of inertia are small and thus $E_{\rm yrast}(J)$ rises rapidly with spin. In particular, $E_{\rm yrast}$ has a strong influence on the heavier fragments, such as α particles, which can remove large amounts of spin. For these particles, the functional form of $E_{\rm yrast}(J)$ can make significant modifications to the predicted shape of the evaporation spectrum in the exponential tail and even in the Coulomb barrier region. The effect of $E_{\rm yrast}$ can be disentangled from the effects of the level-density parameter and the transmission coefficients by comparing data for a lighter particle such as a proton to that for a heavier particle such as an α particle.

In the following three sections, the parametrization of these three ingredients needed to describe experiment data is described. We discuss light and heavy systems separately.

IV. HEAVY COMPOUND NUCLEI

Let us start by concentrating on the heavier compound nuclei with $A > 150$, for which the evaporation spectra are shown in Figs. 1 to 5. These data sets were all obtained with a coincidence requirement of a detected evaporation residue. We first consider which transmission coefficients and level densities allow us to reproduce the shape of the experimental spectra. Predicted spectra in these figures are normalized to give the same peak differential multiplicity to concentrate of the reproduction the spectral shapes. Subsequently, we return to consider how well one can reproduce the absolute multiplicities of evaporated protons and α particles.

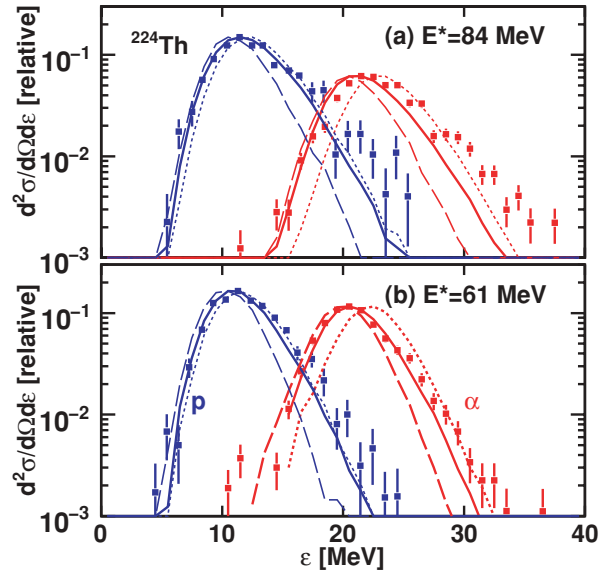

FIG. 1. (Color online) Center-of-mass kinetic-energy spectra of α particles and protons detected in coincidence with evaporation residues formed in ^{16}O + ^{208}Pb reactions. Experimental results (data points) are shown for the indicated excitation energies of the ^{224}Th compound nuclei. The curves show spectra predicted with the GEMINI++ code and normalized to the same peak height as the experimental data. The solid curves (the default calculations of the code) were obtained with the excitation-dependent level-density parameter and with distributions of Coulomb barriers. The short-dashed curves indicated the results obtained using a single Coulomb barrier and the long-dashed curves are associated with an excitation-independent $\widetilde{a} = A/7.3$ MeV^{-1} level-density parameter.

A. Transmission coefficients

The evaporation formalism is justified on the condition of detailed balance. The evaporation rate of an isolated CN is assumed to be identical to the emission rate of such a nucleus in equilibrium with a gas of the evaporated particles. In equilibrium there is a balance between the emission and the inverse, absorption rates of that particle and thus the transmission coefficients or barrier penetration probabilities should be identical to those for the inverse absorption process.

Transmission coefficients have traditionally been obtained from the inverse reaction using optical-model parameters obtained from global optical-model fits to elastic-scattering data. There are two problems with this approach. First, Alexander *et al.* [37] have pointed out that such transmission coefficients contain the effects of transparency in the inverse reaction, which is not appropriate in evaporation. Instead, is was suggested that the real optical-model potentials should still be used, but to ensure full absorption, the incoming-wave boundary-condition (IWBC) model [38] be used to calculate T_ℓ. In GEMINI++, global optical-model potentials were obtained from Refs. [39–45]. The difference between IWBC and optical-model transmission coefficients is only

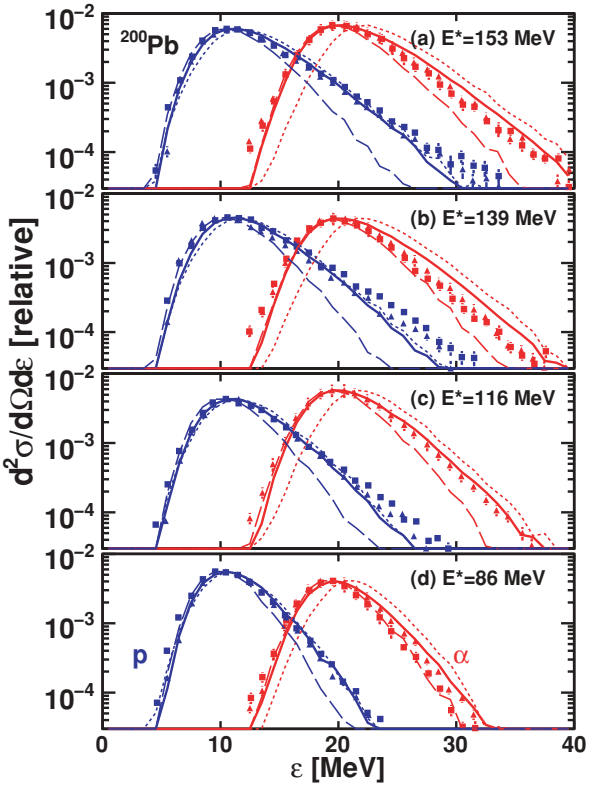

FIG. 2. (Color online) As in Fig. 1, but now for ^{200}Pb compound nuclei formed in ^{19}F + ^{181}Ta reactions.

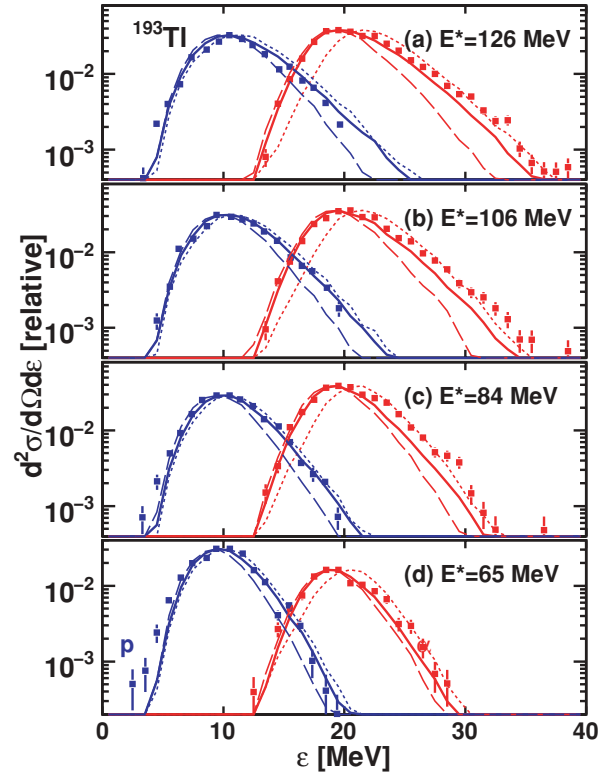

FIG. 3. (Color online) As in Fig. 1 but now for ^{193}Tl compound nuclei formed in ^{32}Si + ^{160}Ho reactions.

important for neutrons, protons, deuterons, tritons, and ^{3}He particles as other particles experience strong absorption inside the Coulomb barrier. Owing to transparency, optical-model transmission coefficients for nucleons do not approach unity for energies well above the barrier, as is the case for the IWBC values. However, the difference between IWBC and standard optical-model T_ℓ values is not that large and it is difficult to differentiate them based on experimental data owing to uncertainties in other statistical-model parameters. Comparisons of statistical-model predictions with IBWC and standard optical-model values of T_ℓ are made in Refs. [20,46], where the biggest differences are associated with deuteron and triton spectra.

The more important problem with the traditional transmission coefficients is that they are not associated with the inverse reaction. The true inverse process to evaporation is the absorption of the particle by a hot, rotating target nucleus which is impossible to measure experimentally. This is highlighted by the fact that IWBC and optical-model transmission coefficients fail to reproduce the shape of the low-energy or "sub-barrier" region of the spectra of α and other heavier particles [5,6,20,26,27,47–49]. We illustrate this in Figs. 1 to 5 where statistical-model predictions obtained with GEMINI++ using the IWBC transmission coefficients, indicated by the short-dashed curves, are compared to experimental data. The level-density prescription used in these calculations are described in the following sections, and Sierk's values of $E_{\rm yrast}$ were used. For α particles emitted from these heavier systems, the relative yield in the sub-barrier region is clearly underpredicted.

Some studies have attempted to reproduce such data by reducing the Coulomb barrier, for example, by allowing an extended radial-profile of a spherical nucleus [50]. However, a simple reduction in the barrier, just shifts the kinetic-energy spectrum down in energy. The experimental α-particle spectra have more rounded maxima than predictions with such barriers. This is illustrated in Fig. 6, where the α spectrum measured for $E^* = 120$-MeV ^{193}Tl compound nuclei formed in ^{28}Si + ^{160}Ho reactions is compared to a number of calculations. The solid curve is again the prediction with the standard IWBC transmission coefficients. For the short-dashed curve, the Coulomb barrier was decreased by increasing the radius parameter of the nuclear potential by δr from its original value of R_0 in the global optical-model potential. The value of δr is temperature dependent and is given later. With the reduced barrier, there is a predicted increase in the yield at lower energies but the yield starts dropping too early with energy and does not reproduce the width of the experimental distribution. For interest's sake, the spectrum predicted with $R_0 - \delta r$ is indicated by the long-dashed curve. Although decreasing the level-density parameter will increase the predicted width of the spectrum, the exponential slope of the experimental spectrum is already reproduced for $E_{\rm c.m.} > 27$ MeV by all the curves. It is clear that if one considered a distribution of radius parameters, one could increase the predicted width of the α-particle spectrum. This conclusion was also found for evaporated Li and Be particles [51].

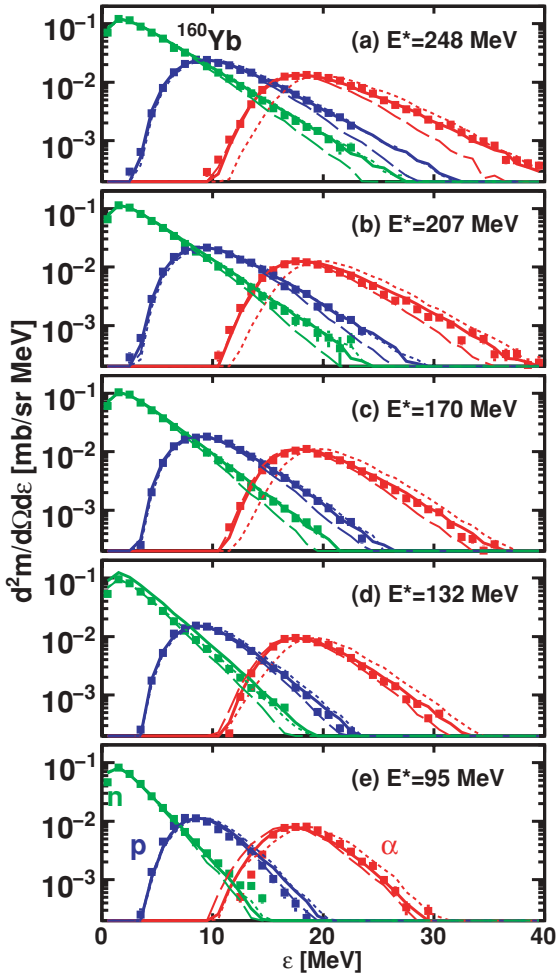

FIG. 4. (Color online) As in Fig. 1 but now for ^{160}Yb compound nuclei formed in ^{60}Ni + ^{100}Mo reactions with neutron spectra also included.

A distribution could arise from a static nuclear deformation if evaporation is averaged over the nuclear surface [52]. Alternatively, the origin of this distribution may have contributions from CN thermal shape fluctuations [53,54] and/or fluctuation in the diffuseness of the nuclear surface or nuclear size.

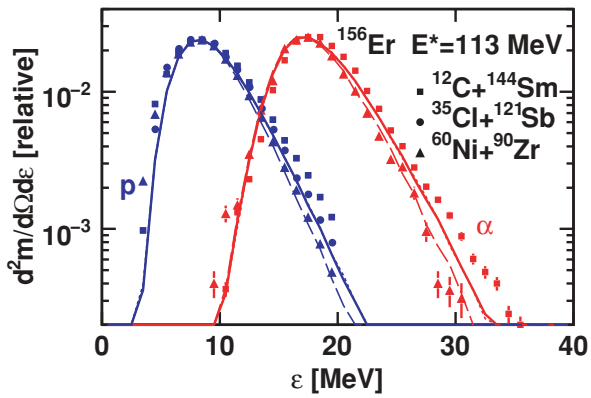

FIG. 5. (Color online) As in Fig. 1 but now for ^{156}Er compound nuclei formed in the three indicated reactions.

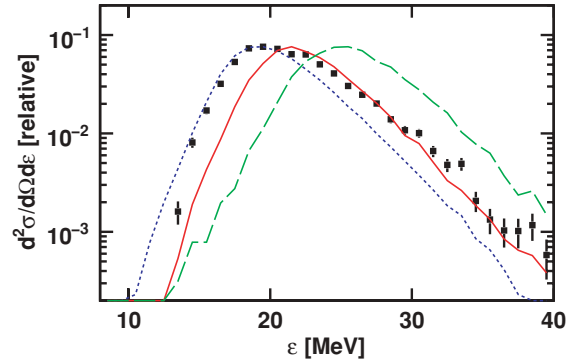

FIG. 6. (Color online) Comparison of the experimental α-particle evaporation spectrum (data points) measured in the ^{28}Si + ^{160}Ho reaction producing ^{193}Tl compound nuclei at $E^* = 126$ MeV to GEMINI++ predictions. The solid curve was obtained with standard IWBC transmission coefficients, while the short- and long-dashed curves were obtained by increasing and decreasing the radius parameter of the nuclear potential, respectively (see text). The curves have been normalized to the same peak height as the experimental data.

If the fluctuations are thermally induced, then we expect, to first order, their variance to be proportional to temperature. In GEMINI++, a simple scheme was implemented to incorporate the effects of barrier distributions. The transmission coefficients were calculated as

$$T_\ell(\varepsilon) = \frac{T_\ell^{R_0-\delta r}(\varepsilon) + T_\ell^{R_0}(\varepsilon) + T_\ell^{R_0+\delta r}(\varepsilon)}{3}, \tag{9}$$

which is the average of three IWBC transmission coefficients calculated with three different radius parameters of the nuclear potential. It was assumed that

$$\delta r = w\sqrt{T}, \tag{10}$$

consistent with thermal fluctuations where the value of the parameter $w = 1.0$ fm was obtained from fits to experiment data and T is the nuclear temperature of the daughter nucleus as defined in Eq. (8). An example of these transmission coefficients is shown in Fig. 7 for $\alpha + ^{193}$Tl with $\ell = 0$

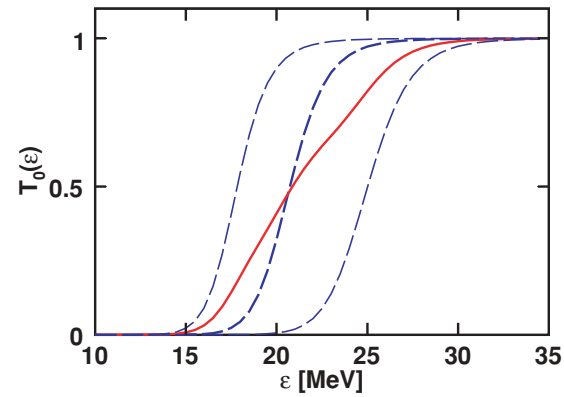

FIG. 7. (Color online) Transmission coefficents for $\alpha + ^{193}$Tl at $\ell = 0$. The dashed curves show the three transmission coefficients of different nuclear radii which are averaged in Eq. (9) and the solid curve is the result.

at $T = 3$ MeV. The dashed curves show three transmission coefficients associated with the three radii in Eq. (9) and the solid curve is the final result, the average of the three dashed curves. The more gradual rise of the transmission with kinetic energy gives rise to a broader peak in the predicted α-particle spectra.

Results obtained with this prescription are indicated by the solid curves in Figs. 1 to 5 and generally reproduce the α particle data quite well.

Because of their lower absolute Coulomb barriers, the effect of the distribution is much less for protons and is practically absent for neutrons. However, the agreement for protons is generally improved.

One should note that the magnitudes of the fluctuations are very large. For a temperature of $T = 3$ MeV, δr is $\sim$25% of the nuclear radius for $A = 160$. For ellipsoidal shape fluctuations in Ref. [51], the full width at half maximum of the Coulomb barrier distributions was predicted to be only $\sim$7%. This suggests that either higher-order shape fluctuations are required or the fluctuations are associated with density profile.

The effects of the barrier distributions is to increase the width of the kinetic-energy window around the barrier where the transmission coefficients change significantly. For example, in Fig. 7, the transmission coefficient changed from 10% to 90% over an interval of 4.5 MeV for IWBC calculation $[T_\ell^{R_0}(\epsilon)]$. However, with Eq. (9), this increased to 9.2 MeV. An alternative way of increasing the width of this window would be to make the radial width of the barrier narrower. Narrow barriers allow for more tunneling and enhance the transmission just below the barrier and also decrease it just above the barrier. However, it is difficult to see how the barrier could be made significantly narrower as the decrease in the potential at large distances is dictated by the Coulomb potential, which falls off slowly. Thus, barrier distributions are the most likely explanation.

B. Level-density parameter

The slope of the exponential tail of the kinetic-energy spectrum gives sensitivity to the nuclear temperature T [Eq. (8)]. The temperature is dependent on the rate of change of the level density, but not its absolute value.

The Fermi-gas level-density prescription of Sec. III can be further refined by including the pairing interaction [55,56]. For the spin and excitation-energy region of interest in this work, the pairing gap has vanished and we can use a backshifted Fermi-gas formula by substituting the following definition of the thermal excitation energy:

$$U = E^* - E_{\text{yrast}}(J) + \delta P, \tag{11}$$

where δP is the pairing correction to the empirical mass formula.

At low excitation energies, the absolute level density can be measured via neutron-resonance counting. The level-density parameters extracted from such data in Ref. [57], using the backshifted Fermi-gas formula, are plotted in Fig. 8. The level-density parameter has strong fluctuations owing to shell

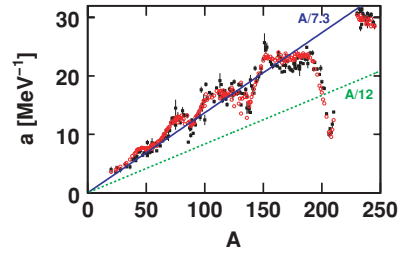

FIG. 8. (Color online) Mass dependence of level-density parameters. Experimental points from neutron-resonance counting are shown as the solid square data points. The open circles are fits obtained using Eq. (12).

effects, which can be parametrized as [58]

$$a(U) = \tilde{a}\left[1 - h(U/\eta + J/J_\eta)\frac{\delta W}{U}\right], \tag{12}$$

where δW is the shell correction to the liquid-drop mass and $\tilde{a}$ is a smoothed level-density parameter. With $h(x) = \tanh(x)$, we obtain a best fit (open circles) to the experimental data with $\eta = 19$ MeV and $\tilde{a} = A/7.3$ MeV^{-1}.

The angular-momentum dependence of $h(x)$ is irrelevant for neutron resonances which are S wave in nature. However, for fusion reactions, it was decided to include a fading out of shell effects with spin. Although at high spins and low values of U, shell corrections are still important, the configuration of the nucleus has changed from the ground state and the use of the ground-state shell correction is wrong. Rather than use an incorrect shell correction, it was decided to use no correction at all. The parameter J_η was set to 50 $\hbar$.

The preceding prescription for the fadeout of shell and pairing corrections is used in all GEMINI++ calculations with separation energies B_i, nuclear masses, shell δW, and pairing δP corrections obtained from the tabulations of Möller *et al.* [59].

Predicted kinetic-energy spectra obtained using this pairing and shell-modified Fermi-gas level-density prescription are shown as the long-dashed curves in Figs. 1 to 5. They significantly underestimate the yield in the exponential tails for the heavier systems. This disagreement gets worse with both increasing CN mass and increasing excitation energy. These results suggest that an excitation-dependent value of $\tilde{a}$ is needed.

The value of the smoothed level-density parameter $\tilde{a}$ used in these calculations is large compared to estimates from the independent-particle model of $\tilde{a} = A/10 - A/11$ MeV^{-1} [60,61] and the difference has been attributed to correlations. In particular, it is the long-range correlations associated with coupling of nucleon single-particle degrees of freedom to low-lying collective modes and giant resonances that are most important.

It has been proposed that long-range correlations modify the Fermi-gas level density in two ways. The first of these is called collective enhancement [62,63]. For example, if we have a deformed nucleus, then for each single-particle configuration, one can consider collective rotations. In addition, both spherical and deformed nuclei can have collective vibrational motions. These collective motions give rise to

rotational and vibrational bands enhancing the level density above the single-particle value, that is,

$$\rho(E^*) = K_{\rm coll}(E^*)\rho_{\rm FG}(E^*), \tag{13}$$

where $K_{\rm coll}$ is the collective enhancement factor.

Long-range correlations, and to a lesser extent also short-range correlations, cause an enhancement of the single-particle level densities $g^n(\varepsilon_F^n)$ and $g^p(\varepsilon_F^p)$ in Eq. (5) [64], which leads to an enhancement in a. This enhancement is counterbalanced by the effect of nonlocality. In fact, without the correlations, we would expect smaller level-density parameters than the predicted $\widetilde{a} = A/10$–$A/11$ MeV^{-1} values owing to the unbalanced effect of nonlocality. As U increases, long-range correlations are expected to wash out, giving rise to both a disappearance of collective enhancement ($K_{\rm coll} \rightarrow 1$) and a reduction in the level-density parameter itself [62,63,65].

In this work, we interpret level densities through the Fermi-gas formula, that is, take Eq. (4) as correct by definition, but use an effective level-density parameter $\widetilde{a}_{\rm eff}$ that is enhanced above the single-particle estimate of Eq. (5) and decreases with excitation energy owing to the fadeout of these long-range correlations; that is,

$$\rho(E^*) = \rho_{\rm FG}(E^*, \widetilde{a}_{\rm eff}) = K_{\rm coll}(E^*)\rho_{\rm FG}(E^*, \widetilde{a}). \tag{14}$$

At low energies, $\widetilde{a}_{\rm eff}$ is set to the value of $A/7.3$ MeV^{-1} to be consistent with the counting of neutron resonances.

We have parametrized its excitation-energy dependence by

$$\widetilde{a}_{\rm eff}(U) = \frac{A}{k_\infty - (k_\infty - k_0)\exp\left(-\frac{\kappa}{k_\infty - k_0}\frac{U}{A}\right)}, \tag{15}$$

where $k_0 = 7.3$ MeV and the asymptotic value at high excitation energy is $\widetilde{a}_{\rm eff} = A/k_\infty$. The parameter κ defines how fast the long-range correlations wash out with excitation energy. This expression is expected to be valid only to moderately high excitation energies where expansion and increases in the surface diffuseness [65,66] are not significant.

Experimental evidence for an excitation-energy dependence of $\widetilde{a}_{\rm eff}$ was found in the $A \sim 160$ region; measurements of light-particle evaporation spectra (n,p,α) with excitation energies ranging from 50 to 250 MeV [9,25] show clear evidence of a departure from a constant value of $\widetilde{a}_{\rm eff}$, with the data being reproduced by the parametrization

$$\widetilde{a}_{\rm eff}(U) = \frac{A}{k_0 + \kappa U/A}, \tag{16}$$

when $k_0 = 7$ MeV and $\kappa = 1.3$ MeV. This equation is just a lower-order approximation of Eq. (15). From an examination of other studies on evaporation spectra, it is apparent that there is a strong A dependence of κ. Nebbia *et al.* [21] find no deviation from a constant $\widetilde{a}_{\rm eff}$ value for the ^{106}Cd CN with excitation energies up to 291 MeV [21]. Whereas for heavier systems, larger values of κ are deduced, values of $\kappa = 2$–3 were found for $A \sim 200$ ($E^* < 150$ MeV) [26,27] and $\kappa = 8.5$ for $A = 224$ ($E^* < 90$) [26], with $k_0 = 8$ MeV.

In this work, we have made a systematic study of the A dependence of κ by fitting the evaporation spectra with Eq. (15). At the excitation energies studied, we cannot constrain the value of k_∞ and it was set to 12 MeV. The fitted values of κ obtained from reproducing the evaporation spectra

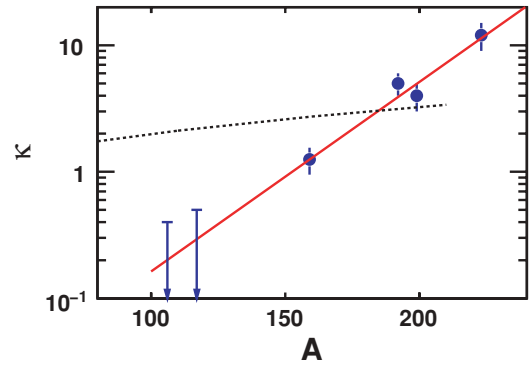

FIG. 9. (Color online) Values of κ in Eq. (15) obtained from fitting evaporation spectra. The solid line shows a smooth approximation used to calculate evaporation spectra and ER excitation functions. The dashed curve shows κ values extracted from the predictions of Ref. [65].

in Figs. 1 to 4 are plotted versus A in Fig. 9. For a single CN, the values of κ obtained from fitting the proton and α spectra were similar, though not always identical, and the error bars in Fig. 9 reflect this range of κ values.

In addition to these data points, Fig. 9 gives some limits for κ obtained from ^{117}Te and ^{106}Cd compound nuclei. These data are, in fact, consistent with $\kappa = 0$ and are discussed in more detail in Sec. V.

Figure 9 is a log plot and it indicates that κ increases very rapidly with mass number. Although we do not have enough data points to determine this dependence in detail, we have fitted it with the exponential function shown by the solid line in this figure and given by

$$\kappa(A) = 0.00517\exp(0.0345A). \tag{17}$$

The excitation-energy dependence of the level-density parameter associated with this dependence is illustrated in Fig. 10 for the indicated A values. The excitation dependence is very strong for the heaviest compound nuclei, but below $A < 100$, there is very little dependence. Statistical-model calculations preformed with this dependence are indicated by the solid curves in Figs. 1 to 5. They reproduce the data much

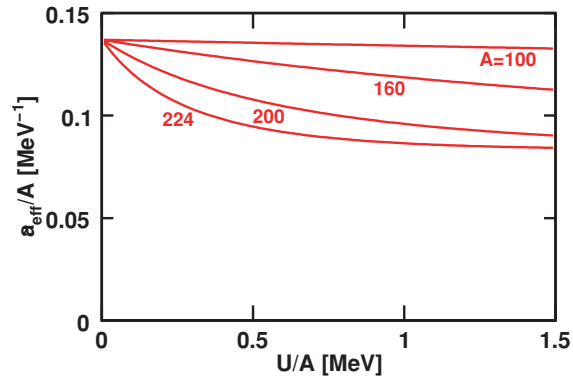

FIG. 10. (Color online) Excitation-energy dependence of the smoothed level-density parameter obtained in this work for the indicated A values.

better than a constant $\widetilde{a}_{\rm eff} = A/7.3$ MeV^{-1}, though they are not perfect.

The individual fits to each reaction (not shown) are slightly better but quite similar. In the similar-mass ^{193}Tl and ^{200}Pb systems, the tails of the α-particle spectra are under- and overpredicted, respectively. This could just be an artifact owing to small experimental errors in the two studies or may reflect an asymmetry $(N - Z)/A$ dependence of κ or even an entrance channel effect. Also, the ^{224}Th data clearly suffer from large statistical errors owing to the very small residue cross sections. Further systematic measurements of a large number of compound nuclei with the same experimental apparatus would help resolve these issues.

More sophisticated calculations of nuclear level density have been obtained within the shell-model Monte Carlo method, but only for light nuclei such as ^{56}Fe have calculations been extended to high excitation energies [67]. These calculated level densities can be fit with a constant level-density parameter of value $A/9.5$ MeV^{-1}. This is basically consistent with the results of this work in that the level density of light nuclei has a Fermi-gas form ($\widetilde{a}_{\rm eff}$ independent of U); however, the value of $A/9.5$ MeV^{-1} is a little smaller than the value $A/7.3$ MeV^{-1} used in this work.

C. Multiplicities and cross sections

So far we have only considered the shapes of the kinetic-energy spectra. It is also important to determine the accuracy to which the absolute yields of evaporated particles can be predicted. For the ^{156}Er, ^{160}Yb, ^{193}Tl, ^{200}Pb, and ^{224}Th compound nuclei for which light particles were detected in coincidence with evaporation residues, the predicted multiplicities are compared to the experimental proton and α-particle values in Figs. 11 and 12. To separate the data from the different systems, the multiplicities were scaled by the indicated amounts. The solid curves in both figures show calculations with the default setting of the code, that is, distribution of Coulomb barriers and an excitation-dependent level-density parameter $\widetilde{a}_{\rm eff}$. They

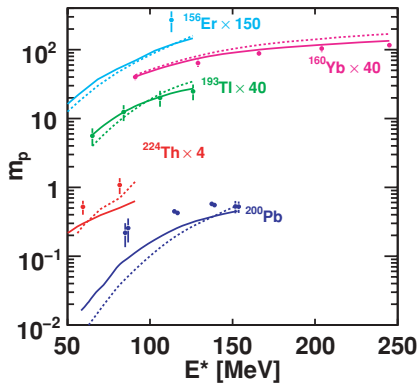

FIG. 11. (Color online) Comparison of experimental and predicted proton multiplicities from the indicated compound nuclei. To aid in viewing, the data have been scaled by the indicated factors. The solid curves were obtained with the excitation-dependent level-density parameter and with distribution of Coulomb barriers. The dashed curves show the prediction with single Coulomb barriers and a constant $\widetilde{a}_{\rm eff} = A/7.3$ MeV^{-1}.

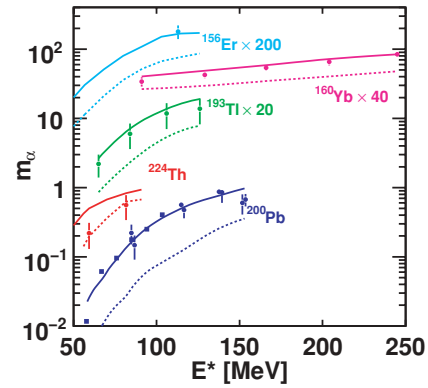

FIG. 12. (Color online) As for Fig. 11 but for α-particle multiplicities.

reproduce the α-particle data quite well. For protons, the ^{160}Yb and ^{193}Tl data are well reproduced, while the other systems underpredict the multiplicities by up to a factor of 2.

It is difficult to understand how a better overall reproduction of the experimental proton multiplicities can be obtained for $A \sim 160$. For example, the ^{156}Er and ^{160}Yb compound nuclei have similar Z and A values, are both produced in Ni induced reactions, and thus explore similar spin distributions. The protons are predicted to be emitted at large excitation energies, where shell and pairing effects are expected to be washed out. Modifications to GEMINI++ that increase the proton multiplicity for the ^{156}Er system will also increase the multiplicities for the ^{160}Yb system in disagreement with the experimental data. One should consider whether the inability to simultaneously fit these two systems is an experimental problem.

These predicted multiplicities are quite sensitive to the level-density and Coulomb barrier prescription. To illustrate this, the dashed curves in Figs. 11 and 12 were obtained with a constant $\widetilde{a}_{\rm eff} = A/7.3$ MeV^{-1} and with the IWBC transmission coefficients for a single Coulomb barrier. For α particles, this results in a large decrease of the multiplicities by a factor of 3 to 10. Clearly, the level density and Coulomb barrier distribution are important to correctly predict these multiplicities. For protons we are somewhat less sensitive to these ingredients.

D. Consequence for fission

Although this work is not focused on the fission probability, it is interesting to determine the consequences of the parametrizations in the preceding sections on the fission probability. Fission was first incorporated into the statistical model by Bohr and Wheeler using the transition-state formalism first introduced to calculate chemical reaction rates. The Bohr-Wheeler decay width [68] is

$$\Gamma_{\rm BW}(E^*, J) = \frac{\pi}{\rho_{\rm CN}(E^*, J)} \int \rho_s(E^* - B_f(J) - \epsilon, J)\, d\epsilon, \tag{18}$$

where $B_f(J)$ is the spin-dependent fission barrier, and ρ_S is the level density at the transition state, that is, the

saddle-point configuration. The variable ϵ is the kinetic energy in the fission degree of freedom at the saddle point. Later, in a one-dimensional diffusion model, Kramers [69] derived a formula similar to this with a different factor before the integral. For large viscosity, the decay width is

$$\Gamma_{\rm Kramers}(E^*, J) = f_k \Gamma_f^{\rm BW}(E^*, J), \tag{19}$$

$$f_k = \sqrt{1 + \left(\frac{\gamma}{2\omega}\right)^2} - \frac{\gamma}{\omega}, \tag{20}$$

where γ is the magnitude of the viscosity and ω is the curvature of the potential energy at the saddle point. The Kramers factor f_k scaling the Bohr-Wheeler width is less than unity and is hard to extract experimentally owing to the much larger uncertainty associated with the fission barrier and the level-density parameter.

The fission decay width has also been suggested to be transient [70], that is, initially zero and then rising to the quasistationary value of Kramers. This idea has helped to explain the large number of neutrons emitted before the scission point is attained [71]. During the transient time, which can also be thought as a fission delay, any light-particle evaporation will lower the excitation energy and spin of the decaying nucleus and subsequently may reduce its fission probability.

However, there is some controversy as to whether transient fission decay widths are needed to explain experimental fission probabilities. A number of theoretical studies reproduce experimental fission probabilities and pre-scission neutron multiplicities with transient fission widths [72,73]. The viscosity which determined the transient time scale was found to increase with the mass in these studies. Transient fission has also been invoked to explain the unexpectedly large number of evaporation residues measured in the very fissile ^{216}Th compound system formed in ^{32}S + ^{184}W reactions [74]. Alternatively, other studies have reproduced fission probabilities [75] and both pre-scission neutron multiplicities and fission probabilities with no transient effects [76]. Similarly, in very-high-excitation-energy data obtained with 2.5-GeV-proton-induced spallation reactions, no transients were needed in reproducing the measured fission yields [77].

In this work, we do not try to answer all these uncertainties pertaining to fission, but investigate how the excitation-dependent level-density parameter affects the fission probability. The fission decay width is taken from the Bohr-Wheeler formalism. Let us assume that the level-density parameter for the saddle-point and ground-state configurations are identical apart from a scaling factor a_f/a_n which accounts for the increased surface area of the former [78]. Fission decay widths were calculated using the angular-momentum-dependent fission barriers of Sierk [36]. For ^{200}Pb, ^{216}Th,^{224}Th, and ^{224}Ra compound nuclei formed in the reactions listed in Table II, both ER and fission excitation functions have been measured, allowing us to determine the fusion cross section and thus constrain the CN spin distributions. Evaporation-residue excitation functions were calculated with the exponential dependence of κ in Fig. 9 and some final adjustment was made with the parameter a_f/a_n to reproduce the experimental data. The results, shown by the solid curves in Fig. 13, reproduce the data quite well and the fitted a_f/a_n values, which are all similar in magnitude, are listed in Table II. For comparison, the short-dashed curves show the results obtained with a constant $\tilde{a}_{\rm eff} = A/7.3\,{\rm MeV}^{-1}$. The U dependence of $\tilde{a}_{\rm eff}$ gives rise to an enhancement of the predicted ER yield which is most pronounced for the heavier systems and the higher excitation energies. However, for the energy regime where there is significant enhancement, the fission cross sections are orders of magnitude larger and even with this enhancement, ER survival is still a rare process.

TABLE II. Experimental data used in Fig. 13 are listed with the CN, reaction, references and a_f/a_n values used in the GEMINI++ calculations.

CN	Reaction	Ref.	a_f/a_n
^{200}Pb	^{19}F + ^{181}Ta	[27,79,80]	1.04
^{216}Ra	^{19}F + ^{197}Au	[81]	1.04
^{216}Th	^{32}S + ^{184}W	[74,82]	1.06
^{224}Th	^{16}O + ^{208}Pb	[26,28–30]	1.035

The calculations with the excitation-dependent values of $\tilde{a}_{\rm eff}$ have higher nuclear temperatures than the $A/7.3$ MeV^{-1} calculation. Larger temperatures enhance rare decay modes and these rare decay modes are the evaporation channels in these very fissile nuclei. This is illustrated by the long-dashed curves which are calculations with a constant $\tilde{a}_{\rm eff} = A/11$ MeV^{-1}, where the temperatures are 20% larger than for $\tilde{a}_{\rm eff} = A/7.3$ MeV^{-1}. These curves also show enhanced evaporation residue yields, but the excitation-energy dependence is not as well described as by the solid curves with the excitation-energy dependence. For the ^{216}Th system of Fig. 13(a), Back *et al.*, using calculations with constant $\tilde{a}_{\rm eff}$, concluded that the statistical model was not able to reproduce the data and thus deduced that there must be fission transients [30]. However, it is now clear that with an excitation-energy-dependent $\tilde{a}_{\rm eff}$, this conclusion is no longer valid. This suggests the possibility of a reduced role for fission transients in determining the fission probability.

It should be noted that the ability of these calculations to reproduce the evaporation-residue cross sections depends on the

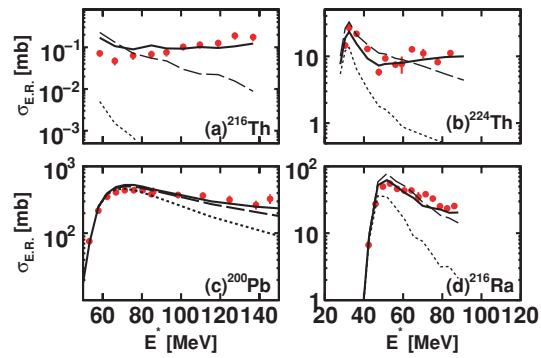

FIG. 13. (Color online) Evaporation-residue excitation functions for the indicated compound nuclei. The data points are published experimental results and the short-dashed, long-dashed, and solid curves were calculated with $\tilde{a}_{\rm eff} = A/7.3$, $\tilde{a} = A/11$ MeV^{-1}, and Eq. (15), respectively.

assumed excitation-energy dependence of $\widetilde{a}_{\rm eff}$. For the lighter ^{160}Yb system of Fig. 4, the excitation-energy dependence is rather well established [25]. A larger range of CN excitation energies were probed (Table I) and neutron evaporation spectra were also measured. Charged particles are typically emitted early the decay chain and probe higher excitation energies, whereas neutrons are emitted at all decay stages and give information more on the average temperature. Reproduction of both charged-particle and neutron spectra required an excitation-energy dependence of $\widetilde{a}_{\rm eff}$ for ^{160}Yb. Subsequently, these $\widetilde{a}_{\rm eff}$ values were found to be consistent with data from the similar-mass ^{178}Hf compound nuclei at even lower excitation energies [9]. By contrast only charge-particle spectra were measured for the ^{224}Th CN in Ref. [26] and at just two excitation energies separated by ∼20 MeV. It also was possible to fit these spectra with a constant $\widetilde{a}_{\rm eff} = A/15$ MeV^{-1} [26]. Although a constant value is unlikely given the larger values derived from counting neutron resonances, it is clear that for this heavy nucleus, the excitation dependence of $\widetilde{a}_{\rm eff}$ is not well constrained from the present experimental data. Clearly, further experimental studies of this point would be useful in understanding the fission in these very heavier systems. Also, it should be noted that for $A \sim 220$, quasifission also competes with fusion reactions at the lower ℓ waves associated with evaporation-residue production for entrance channels with ^{19}F projectiles and heavier [81,83]. This suggests that somewhat smaller values of a_f/a_n are associated with the ^{19}F + ^{197}Au and ^{32}S + ^{184}W reactions than those of Table II.

Finally, it is of interest to consider the relevance of this work to the production of superheavy elements. Of particular interest are "hot" fusion reactions which have produced the heaviest elements to date [84,85]. Based on an extrapolation of κ to the $A = 277$–294 region, we would expect significantly enhanced temperatures for the CN excitation energies of ∼35 MeV produced in these reactions. Therefore, this effect may also contribute to an enhanced yield of superheavy elements in these hot fusion reactions. Clearly, more studies are also needed in this area.

E. Thermal properties of nuclei

The thermal properties of nuclei can be inferred from the level density [34]. Figures 14(a) and 14(b) show the excitation-energy dependence of S and T plotted in a manner that the mass dependence would disappear for an energy-independent $\widetilde{a}_{\rm eff} \propto A$. The curves for different masses are only plotted up to the maximum U sampled in the experiments. We see a small mass dependence of S/A but a larger dependence for the temperature. For a given U/A, we see smaller values of S/A and larger temperatures for the heavier systems. The larger temperatures are responsible for the stiffer evaporation spectra and the enhancements of the small ER survival probabilities.

The theoretical understanding of the rapid increase in κ with A is not clear. Shlomo and Natowitz [65] assumed the effects of long-range correlations wash out when T becomes similar in magnitude to the collective energy $\hbar\omega_i$ of each of the modes. For many collective modes, ω_i varies approximately inversely with the linear dimension; that is, $\omega_i \sim A^{-1/3}$. Values of κ extracted from the predictions of Shlomo and Natowitz [65], shown by the dashed curve in Fig. 9, have only a gentle mass dependence and do not reproduce our experimental points.

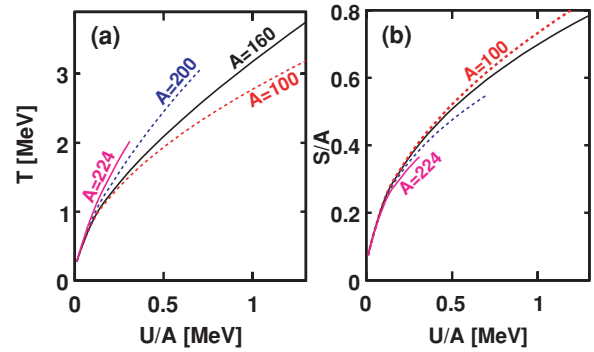

FIG. 14. (Color online) Excitation-energy dependence of (a) the nuclear temperature and (b) the entropy deduced in this work.

V. LIGHTER NUCLEI AND YRAST ENERGIES

Owing to the exponential-like dependence of κ on mass, it seems that the kinetic-energy spectra should be described by an excitation-independent level-density parameter $\widetilde{a}_{\rm eff}$ for the lighter nuclei. However, light nuclei have their own complications because the spin dependence of $E_{\rm yrast}$ can be quite strong. This can cause quite pronounced effects on the predicted spectra of α particles which can remove appreciable angular momentum from the decaying system. Such effects can in principle be isolated if both proton or neutron spectra are also measured because nucleons tend to remove very little angular momentum and thus are much less sensitive to $E_{\rm yrast}$. However, for the lightest nuclei, there are a lot more data available for α particles than protons.

Let us concentrate on the spectra for $A = 117$–59 compound nuclei in Figs. 15 to 19. GEMINI++ calculations including the distribution of Coulomb barriers, Sierk's values of $E_{\rm yrast}$, and the excitation-energy-dependent level-density parameter are indicated by the long-dashed curves. Calculations with a constant $\widetilde{a}_{\rm eff} = A/7.3$ MeV^{-1} would be essentially identical to these. For protons with minimal angular-momentum effects, one obtained good agreement with experimental data for the ^{117}Te, ^{106}Cd, and ^{96}Ru compound systems in Figs. 15 to 17. For the ^{67}Ga system, the proton spectra are not very well reproduced in Figs. 18(b) and 18(c). Actually it is difficult to understand the evolution of the slope of the exponential tails of these proton spectra with excitation energy within the statistical model. The possibility exits that there are experimental problems here or there is contamination from other processes. In fact, for all these lighter nuclei the possibility of contamination exists because the data are all inclusive.

Consider the ^{59}Cu data from the ^{32}S + ^{27}Al reaction in Fig. 19. The evaporation-residue cross section represents about 85% of the total reaction cross section at $E_{\rm beam} = 100$ MeV ($E^* = 58$ MeV) but decreases to 46% at $E_{\rm beam} = 214$ MeV ($E^* = 110$ MeV) [86]. The remaining component of the reaction cross section is associated with binary-reaction dynamics with various degrees of damping and these binary-reaction products evaporate protons and α particles [87–89]. Very

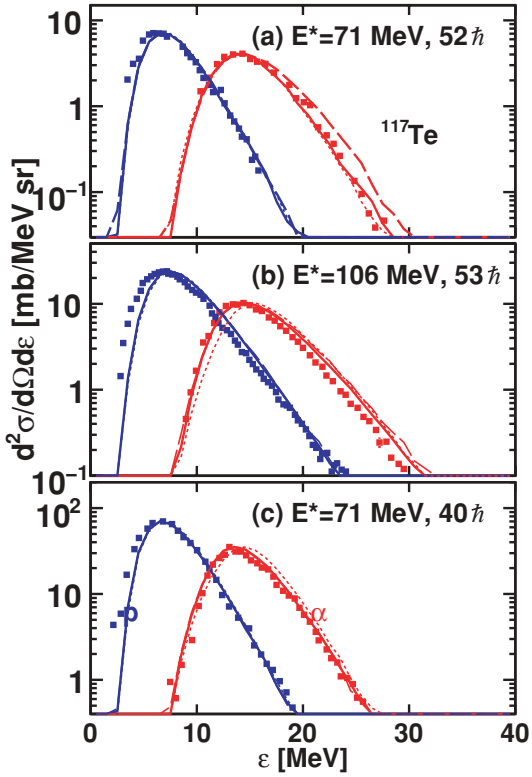

FIG. 15. (Color online) Inclusive proton and α-particle kinetic-energy spectra in the reaction center-of-mass frame measured at angles that highlight CN emission. The data are associated with ^{117}Te CN formed in (a,b) ^{14}N + ^{103}Rh and (c) ^{40}Ar + ^{77}Se reactions. The curves are again GEMINI++ predictions. The solid curves are the default calculations with a distribution of Coulomb barriers, the excitation-dependent level-density parameter $\widetilde{a}_{\rm eff}$, and the prescription for $E_{\rm yrast}(J)$. For the short-dashed curves, a single Coulomb barrier is used and for the long-dashed curves, Sierk's values of $E_{\rm yrast}(J)$ are employed.

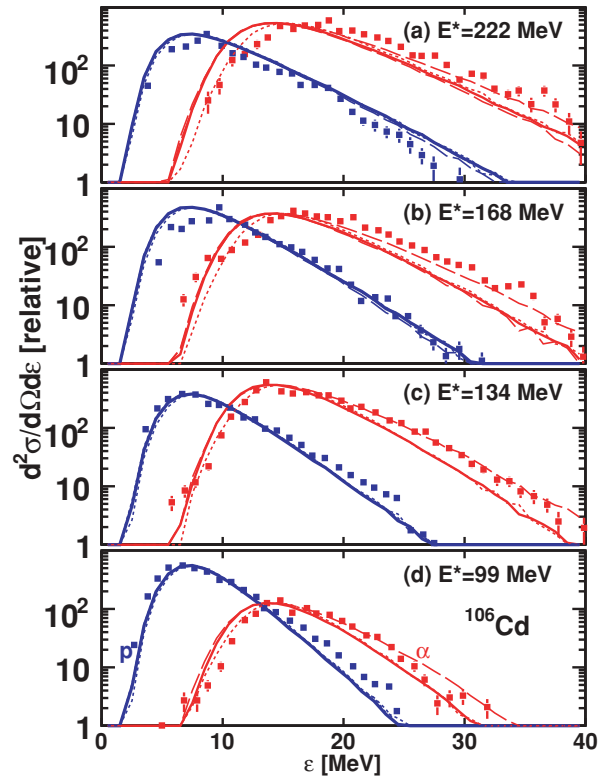

FIG. 16. (Color online) As for Fig. 15 but for ^{106}Cd compound nuclei formed in ^{32}S + ^{74}Ge reactions.

damped binary and fusion-fission reactions are associated with extensive angular distributions and thus light-particle emission from these processes will not have a strong angular distribution and would be difficult to separate from those associated with evaporation residues. Clearly, not all the inclusive α and p spectra can be associated with evaporation, as is assumed in most analyses. The exact extent of this contamination from binary reactions has not been established, but in this work, it is assumed that it is not large for α particles and the basic features of the spectra can be traced to evaporation from the fused system.

For α particles, the GEMINI++ predictions significantly overestimate the yield in the high-energy tail for many of the data sets. In fact, these predicted spectra do not have exponential tails in the sense that the spectral tails decrease linearly on a log plot. This is an indication that the predicted enhancement of the high-energy region is not a consequence of high temperatures, but of angular-momentum effects associated with the steep increase of $E_{\rm yrast}$ with J. The angular-momentum effects are most pronounced for the more symmetric reactions such as the ^{40}Ar + ^{27}Al reactions in Figs. 18(a) and 18(c), which populate a region of E^*-J space near the yrast line at high spins. One also finds the same for the higher-energy ^{32}S + ^{27}Al reactions in Fig. 19.

A large number of previous studies have noted that calculations with Sierk's or the RLDM values of $E_{\rm yrast}$ are incapable of reproducing α-particle spectra from light systems with large angular momentum [12,17–20,52,90–92].

Huizenga *et al.* [52] reproduced experimental α-particle spectra by using a modified yrast energy given by

$$E_{\rm yrast}(J) = \frac{\hbar^2}{2\mathcal{I}_{\rm rig}}(1 + \delta_1 J^2 + \delta_2 J^4), \qquad (21)$$

which contains two free parameters, δ_2 and δ_4, adjusted for each CN. Equally good fits to the data can be obtained by

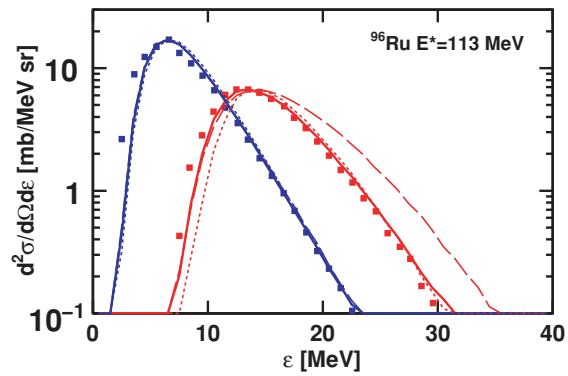

FIG. 17. (Color online) As for Fig. 15 but for ^{96}Ru compound nuclei formed in ^{32}S + ^{64}Ni reactions.

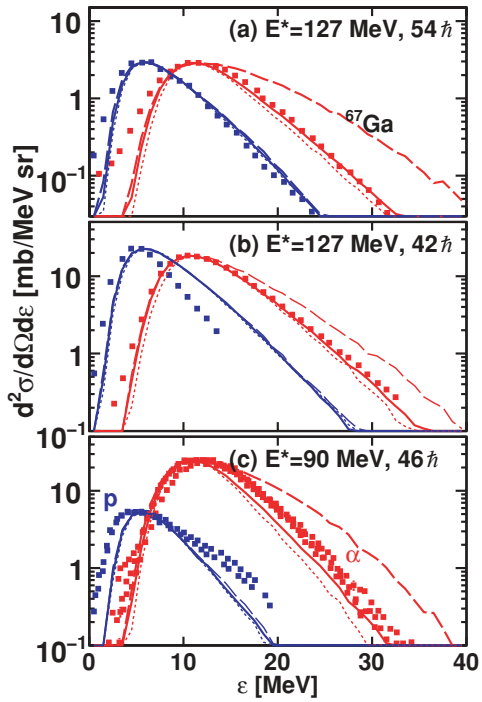

FIG. 18. (Color online) As for Fig. 15 but for ^{67}Ga compound nuclei formed in ^{40}Ar + ^{27}Al and ^{55}Mn + ^{12}C reactions.

using the Sierk calculations out to an angular momentum J_* and subsequently allowing $E_{\rm yrast}(J)$ to increase linearly for higher spins, that is,

$$E_{\rm yrast}(J) = \begin{cases} E_{\rm Sierk}(J), & \text{if} \quad J < J_*, \\ E_{\rm Sierk}(J_*) + (J - J_*)E'_{\rm Sierk}(J_*), & \text{if} \quad J > J_*. \end{cases} \tag{22}$$

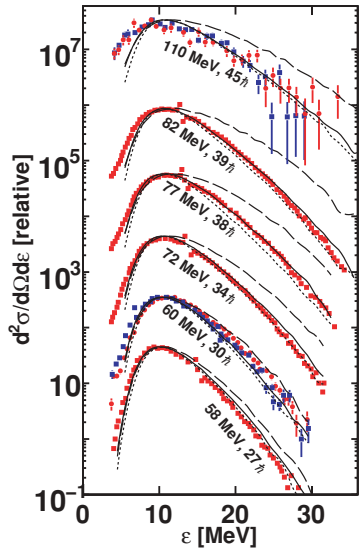

FIG. 19. (Color online) As for Fig. 18, but now for ^{59}Cu compound nuclei. For the $E^* = 60$-MeV data, the square and circular data points represent the results measured at $\theta_{\rm lab} = 25^\circ$ and 45°, respectively, while for the 110-MeV data they correspond to $\theta_{\rm lab} = 15^\circ$ and 30°.

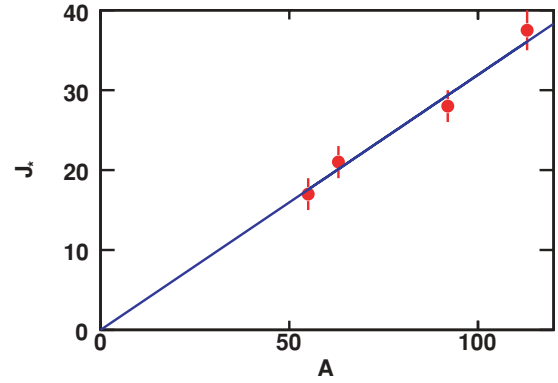

FIG. 20. (Color online) Values of J_*, the angular momentum for which the Sierk yrast energy is modified, are plotted again the mass of the first α-daughter nucleus. The line shows a fit to these values which is used in subsequent GEMINI++ calculations.

This has the advantage of having only one free parameter, making interpolation and extrapolation easier. Also with increasingly large values of J_*, the effect turns off as Sierk's calculations become more linear (see later). In addition, if J_* is made larger than the input CN spin distribution, it has no effect. Thus, if J_* increases with A, it allows a smooth transition to a heavier nucleus where Sierk's values can reproduce experimental data.

The value of J_* was obtained from fits to the data from ^{59}Cu, ^{67}Ga, ^{96}Ru, and ^{117}Te compound nuclei and the values are plotted against the A of the α-daughter system in Fig. 20. These data points can be fit with the linear function

$$J_* = 0.319A, \tag{23}$$

shown by the solid line. GEMINI++ predictions with this global parametrization of J_* are shown by the solid curves in Figs. 15 to 19 and reproduce the experimental distributions reasonably well. The exception is for the ^{106}Cd CN, where the original long-dashed calculations in Fig. 16 obtained with Sierk's $E_{\rm yrast}(J)$ values produced a better fit.

In Fig. 21, we compare the modified $E_{\rm yrast}$ energies to Sierk's calculations for ^{63}Cu and ^{55}Co, the daughter nuclei following α evaporation from the ^{67}Ga and ^{59}Cu compound nuclei. In addition are shown values obtained by Huizenga *et al.* obtained from fitting these data with Eq. (21) [52]. Although the values from this work are slightly lower than those of Huizenga *et al.* at the high spins, the most important comparison is that the slopes of $E_{\rm yrast}(J)$ are very similar at these high spins. As mentioned before, evaporation spectra are not sensitive to absolute level density. In this case the calculations are sensitive to the J dependence of ρ, which is dictated by the spin dependence of $E_{\rm yrast}$. The $E_{\rm yrast}$ values of Huizenga would also give good reproduction of the experimental data if they were used in GEMINI++. Evaporation spectra thus give information on the J dependence of $E_{\rm yrast}$.

Huizenga *et al.* also suggested that $E_{\rm yrast}$ at these high spins not be interpreted as just the rotational-plus-deformation energy of the nucleus after shell and pairing effects have vanished. Rather they should be treated as effective values that may take account of other effects such as a spin dependence of

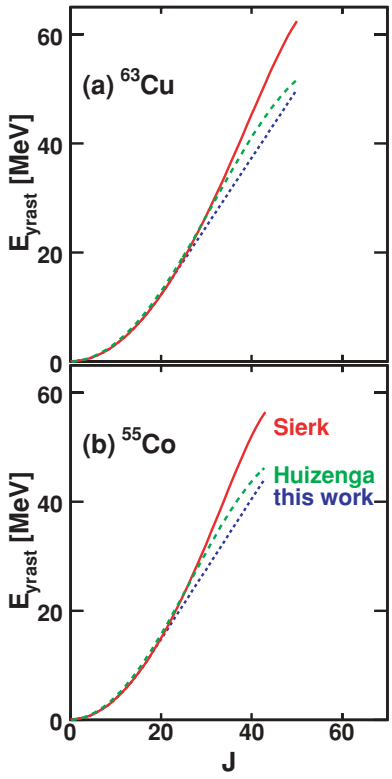

FIG. 21. (Color online) Rotational-plus-deformation energies versus the nuclear angular momentum for (a) ^{63}Cu and (b) ^{55}Co. Curves are shown for the dependence caluculated by Sierk form his macroscopioc model. These can be compared to results obtained from fitting α-particle evaporation spectra in this work and by Huizenga *et al.*

the level-density parameter or spin dependence of collective enhancements.

In Figs. 15 to 19, the short-dashed curves again show the predictions with no barrier distributions in the transmission coefficients. As the absolute barriers are smaller for these lighter nuclei, the effect of the barrier distributions on the spectra are reduced. However, the inclusion of the distributions (solid curves) still improves the agreement with the α-particle data except for the ^{106}Cd CN, where the long-dashed curves give better fits. The ^{106}Cd data has thus proven exceptional in the ingredients necessary to fit both the exponential tails and the Coulomb barrier region. The standard calculations represented by the solid curves in Fig. 16 would fit much better if the experimental spectra were shifted down in energy.

For the ^{59}Cu and ^{67}Ga systems, it is clear that the enhancement from the barrier distributions at the largest excitation energies and J_0 values is not sufficient to reproduce the experimental α-particle spectra in Fig. 19. Again, there are questions about contamination from events not associated with evaporation residues. Majka *et al.* [90] have investigated the need for a J dependence of the transmission coefficients which they associate with the increasing deformation of the equilibrium configuration with spin. At present we have not attempted to modify the transmission coefficients as a function of J in GEMINI++ to better reproduce the data.

For the proton spectra, the inclusion of the barrier distribution practically has no effect. However, the sub-barrier region in ^{117}Te (Fig. 15) and ^{96}Ru (Fig. 17) are still underestimated in the calculations, even though the rest of the spectral shape is well described. Again, there are questions as to whether this is a problem with contamination from other processes. Alternatively, enhancements to the proton sub-barrier region can also arise if the evaporation residue is sufficiently proton rich. If the decay chain of particles leads to a daughter nucleus with excitation energy below the neutron separation energy, but above the proton value, then sub-barrier proton emission competes with γ emission. Such protons are the source of the lowest-energy protons in the GEMINI++ predictions for these systems.

VI. CONCLUSION

A systematic review of the ingredients necessary to describe the shape of proton and α-particle and some neutron evaporation spectra was made. To describe the low-energy yields of the charged particles, transmission coefficients associated with a distribution of barriers were necessary. This was incorporated in a simple way into the statistical model assuming a distribution of barriers which was assumed to arise from large thermal fluctuations. This could include fluctuations in shape, density, or surface diffuseness.

The nuclear level density was described in terms of the Fermi-gas formula, which is valid for single-particle excitations. However, an effective level-density parameter that can also account for collective contributions is used. For light nuclei ($A < 120$), the shell-smoothed values of $\tilde{a} = A/7.3$ MeV^{-1}, obtained from neutron-resonance counting at low excitation energies, were also found consistent with the evaporation spectra. However, for heavier nuclei at large excitation energies, smaller level-density parameters are needed. Evaporation spectra were fit with an excitation-energy-dependent level-density parameter where the excitation-energy dependence increases very rapidly with A. This excitation-energy dependence was also found to be important in understanding the survival against fission in very fissile nuclei and allowed reproduction of data that previously was thought to require fission transients.

The angular-momentum dependence of the level density is largely defined by the spin dependence of the macroscopic yrast energy. For light compound nuclei at large J, modifications to Sierk's and the RLDM values of the rotation-plus-deformation energies which reduce the angular-momentum dependence of the level density were needed to describe experimental α-particle evaporation spectra.

These ingredients were incorporated in the GEMINI++ code to allow a good description of the spectral shape of evaporation spectra over all of the periodic table.

ACKNOWLEDGMENTS

This work was supported by the US Department of Energy, Division of Nuclear Physics, under Grant No. DE-FG02-87ER-40316.

[1] Y. Yariv and Z. Fraenkel, Phys. Rev. C **24**, 488 (1981).
[2] A. Boudard, J. Cugnon, S. Leray, and C. Volant, Phys. Rev. C **66**, 044615 (2002).
[3] L. Ou, Z. Li, X. Wu, J. Tian, and W. Sun, J. Phys. G **36**, 125104 (2009).
[4] M. Cinausero *et al.*, Phys. Lett. B **383**, 372 (1996).
[5] R. J. Charity, M. Korolija, D. G. Sarantites, and L. G. Sobotka, Phys. Rev. C **56**, 873 (1997).
[6] J. F. Liang, J. D. Bierman, M. P. Kelly, A. A. Sonzogni, R. Vandenbosch, and J. P. S. van Schagen, Phys. Rev. C **56**, 908 (1997).
[7] R. J. Charity, in *Joint ICTP-AIEA Advanced Workshop on Model Codes for Spallation Reactions* (IAEA, Vienna, 2008), Report INDC(NDC)-0530.
[8] R. J. Charity *et al.*, Nucl. Phys. A **483**, 371 (1988).
[9] S. Komarov, R. J. Charity, C. J. Chiara, W. Reviol, D. G. Sarantites, L. G. Sobotka, A. L. Caraley, M. P. Carpenter, and D. Seweryniak, Phys. Rev. C **75**, 064611 (2007).
[10] R. Bass, Nucl. Phys. A **231**, 45 (1974); Phys. Rev. Lett. **39**, 265 (1977).
[11] D. Mancusi, R. J. Charity, and J. Cugnon (submitted to Phys. Rev. C., 2010), arXiv:1007.0963 [nucl-th].
[12] B. Fornal, G. Prete, G. Nebbia, F. Trotti, G. Viesti, D. Fabris, K. Hagel, and J. B. Natowitz, Phys. Rev. C **37**, 2624 (1988).
[13] H. H. Gutbrod, W. G. Winn, and M. Blann, Nucl. Phys. A **213**, 267 (1973).
[14] R. L. Kozub, N. H. Lu, J. M. Miller, D. Logan, T. W. Debiak, and L. Kowalski, Phys. Rev. C **11**, 1497 (1975).
[15] F. Pühlhofer, W. F. W. Schneider, F. Busch, J. Barrette, P. Braun-Munzinger, C. K. Gelbke, and H. E. Wegner, Phys. Rev. C **16**, 1010 (1977).
[16] G. Rosner, J. Pochodzalla, B. Heck, G. Hlawatsch, A. Miczaika, H. J. Rabe, R. Butsch, B. Kolb, and B. Sedelmeyer, Phys. Lett. B **150**, 87 (1985).
[17] R. K. Choudhury, P. L. Gonthier, K. Hagel, M. N. Namboodiri, J. B. Natowitz, L. Adler, S. Simon, S. Kniffen, and G. Berkowitz, Phys. Lett. B **143**, 74 (1984).
[18] G. La Rana, D. J. Moses, W. E. Parker, M. Kaplan, D. Logan, R. Lacey, J. M. Alexander, and R. J. Welberry, Phys. Rev. C **35**, 373 (1987).
[19] C. M. Brown, Z. Milosevich, M. Kaplan, E. Vardaci, P. DeYoung, J. P. Whitfield, D. Peterson, C. Dykstra, P. J. Karol, and M. A. McMahan, Phys. Rev. C **60**, 064612 (1999).
[20] M. Kildir *et al.*, Phys. Rev. C **46**, 2264 (1992).
[21] G. Nebbia *et al.*, Nucl. Phys. A **578**, 285 (1994).
[22] J. Galin, B. Gatty, D. Guerreau, C. Rousset, U. C. Schlotthauer-Voos, and X. Tarrago, Phys. Rev. C **9**, 1126 (1974).
[23] J. Galin, B. Gatty, D. Guerreau, C. Rousset, U. C. Schlottauer-Voos, and X. Tarrago, Phys. Rev. C **9**, 1113 (1974).
[24] R. V. F. Janssens, R. Holzmann, W. Henning, T. L. Khoo, K. T. Lesko, G. S. F. Stephans, D. C. Radford, A. M. V. D. Berg, W. Kühn, and R. M. Ronningen, Phys. Lett. B **181**, 16 (1986).
[25] R. J. Charity *et al.*, Phys. Rev. C **67**, 044611 (2003).
[26] B. J. Fineman, K.-T. Brinkmann, A. L. Caraley, N. Gan, R. L. McGrath, and J. Velkovska, Phys. Rev. C **50**, 1991 (1994).
[27] A. L. Caraley, B. P. Henry, J. P. Lestone, and R. Vandenbosch, Phys. Rev. C **62**, 054612 (2000).
[28] F. Videbæk, R. B. Goldstein, L. Grodzins, S. G. Steadman, T. A. Belote, and J. D. Garrett, Phys. Rev. C **15**, 954 (1977).
[29] K.-T. Brinkmann, A. L. Caraley, B. J. Fineman, N. Gan, J. Velkovska, and R. L. McGrath, Phys. Rev. C **50**, 309 (1994).
[30] B. B. Back, R. R. Betts, J. E. Gindler, B. D. Wilkins, S. Saini, M. B. Tsang, C. K. Gelbke, W. G. Lynch, M. A. McMahan, and P. A. Baisden, Phys. Rev. C **32**, 195 (1985).
[31] P. Fröbrich, Phys. Rep. **116**, 337 (1984).
[32] W. Hauser and H. Feshbach, Phys. Rev. **87**, 366 (1952).
[33] L. G. Moretto, Nucl. Phys. A **247**, 211 (1975).
[34] A. Bohr and B. R. Mottleson, *Nuclear Structure* (Benjamin, New York, 1975), Vol. I.
[35] S. Cohen, F. Plasil, and W. J. Swiatecki, Ann. Phys. (NY) **82**, 557 (1974).
[36] A. J. Sierk, Phys. Rev. C **33**, 2039 (1986).
[37] J. M. Alexander, M. T. Magda, and S. Landowne, Phys. Rev. C **42**, 1092 (1990).
[38] G. H. Rawitscher, Nucl. Phys. **85**, 337 (1966).
[39] C. M. Perey and F. G. Perey, Phys. Rev. **132**, 755 (1963).
[40] F. G. Perey, Phys. Rev. **131**, 745 (1963).
[41] D. Wilmore and P. E. Hodgson, Nucl. Phys. **55**, 673 (1964).
[42] L. McFadden and G. R. Satchler, Nucl. Phys. **84**, 177 (1966).
[43] F. D. Becchetti Jr. and G. W. Greenlees, *Polarization Phenomena in Nuclear Reactions* (University of Wisconsin Press, Madison, 1971).
[44] J. Cook, Nucl. Phys. A **388**, 153 (1982).
[45] R. Balzer, M. Hugi, B. Kamys, J. Lang, R. Müller, E. Ungricht, J. Unternährer, L. Jarczyk, and A. Strzałkowski, Nucl. Phys. A **293**, 518 (1977).
[46] M. Kildir *et al.*, Phys. Rev. C **51**, 1873 (1995).
[47] N. G. Nicolis *et al.*, Phys. Rev. C **41**, 2118 (1990).
[48] M. Gonin *et al.*, Phys. Rev. C **42**, 2125 (1990).
[49] J. Boger, J. M. Alexander, R. A. Lacey, and A. Narayanan, Phys. Rev. C **49**, 1587 (1994).
[50] R. Lacey *et al.*, Phys. Lett. B **191**, 253 (1987).
[51] R. J. Charity *et al.*, Phys. Rev. C **63**, 024611 (2001).
[52] J. R. Huizenga, A. N. Behkami, I. M. Govil, W. U. Schröder, and J. Tõke, Phys. Rev. C **40**, 668 (1989).
[53] R. J. Charity, Phys. Rev. C **61**, 054614 (2000).
[54] R. J. Charity, Phys. Rev. C **64**, 064610 (2001).
[55] M. Santo and S. Yamasaki, Prog. Theor. Phys. **29**, 397 (1963).
[56] L. G. Moretto, Nucl. Phy. A **185**, 145 (1972).
[57] B. John, R. K. Choudhury, B. K. Nayak, A. Saxena, and D. C. Biswas, Phys. Rev. C **63**, 054301 (2001).
[58] A. V. Ignatyuk, G. N. Smirenkin, and A. S. Tishin, Sov. J. Nucl. Phys. **21**, 255 (1975).
[59] P. Möller, J. R. Nix, W. D. Myers, and W. J. Swiatecki, At. Data Nucl. Data Tables **59**, 185 (1995).
[60] A. V. Ignatyuk, M. G. Itkis, V. N. Okolovich, G. N. Smirenkin, and A. S. Tishin, Sov. J. Nucl. Phys. **21**, 612 (1976).
[61] R. J. Charity and L. G. Sobotka, Phys. Rev. C **71**, 024310 (2005).
[62] S. Bjørnholm, A. Bohr, and B. R. Mottelson, in *Proceedings of the International Conference on the Physics and Chemistry of Fission, Rochester, New York, 1973* (IAEA, Vienna, 1974), Vol. 1, p. 367.
[63] G. Hansen and A. S. Jensen, Nucl. Phys. A **406**, 236 (1983).
[64] C. Mahaux and R. Sartor, Adv. Nucl. Phys. **20**, 1 (1991).
[65] S. Shlomo and J. B. Natowitz, Phys. Rev. C **44**, 2878 (1991).
[66] L. G. Sobotka and R. J. Charity, Phys. Rev. C **73**, 014609 (2006).
[67] Y. Alhassid, G. F. Bertsch, and L. Fang, Phys. Rev. C **68**, 044322 (2003).
[68] N. Bohr and J. A. Wheeler, Phys. Rev. **56**, 426 (1939).
[69] H. A. Kramers, Physica **7**, 284 (1940).
[70] P. Grangé, L. Jun-Qing, and H. A. Weidenmüller, Phys. Rev. C **27**, 2063 (1983).

[71] D. Hilscher and H. Rossner, Ann. Phys. (Paris) **17**, 471 (1992).
[72] P. Fröbrich, I. I. Gontchar, and N. D. Mavlitov, Nucl. Phys. A **556**, 281 (1993).
[73] I. I. Gontchar and N. E. Aktaev, Phy. Rev. C **80**, 044601 (2009).
[74] B. B. Back, D. J. Blumenthal, C. N. Davids, D. J. Henderson, R. Hermann, D. J. Hofman, C. L. Jiang, H. T. Penttilä, and A. H. Wuosmaa, Phys. Rev. C **60**, 044602 (1999).
[75] L. G. Moretto, K. X. Jing, R. Gatti, G. J. Wozniak, and R. P. Schmitt, Phys. Rev. Lett. **75**, 4186 (1995).
[76] J. P. Lestone and S. G. McCalla, Phys. Rev. C **79**, 044611 (2009).
[77] V. Tishchenko, C.-M. Herbach, D. Hilscher, U. Jahnke, J. Galin, F. Goldenbaum, A. Letourneau, and W.-U. Schröder, Phys. Rev. Lett. **95**, 162701 (2005).
[78] J. Tōke and W. Świątecki, Nucl. Phys. A **372**, 141 (1981).
[79] D. J. Hinde, J. R. Leigh, J. O. Newton, W. Galster, and S. Sie, Nucl. Phys. A **385**, 109 (1982).
[80] D. Fabris *et al.*, Phys. Rev. C **50**, R1261 (1994).
[81] A. C. Berriman, D. J. Hinde, M. Dasgupt, C. R. Morton, R. D. Butt, and J. O. Newton, Nature (London) **413**, 144 (2001).
[82] J. G. Keller, B. B. Back, B. G. Glagola, D. Henderson, S. B. Kaufman, S. J. Sanders, R. H. Siemssen, F. Videbaek, B. D. Wilkins, and A. Worsham, Phys. Rev. C **36**, 1364 (1987).
[83] R. Rafiei, R. G. Thomas, D. J. Hinde, M. Dasgupta, C. R. Morton, L. R. Gasques, M. L. Brown, and M. D. Rodriguez, Phys. Rev. C **77**, 024606 (2008).
[84] Y. T. Oganessian *et al.*, Phys. Rev. C **70**, 064609 (2004).
[85] Y. T. Oganessian, Phys. Scr., T **125**, 57 (2006).
[86] G. Doukellis, G. Hlawatsch, B. Kolb, A. Miczaika, G. Rosner, and B. Sedelmeyer, Nucl. Phys. A **485**, 369 (1988).
[87] U. Winkler, R. Giraud, H. Gräf, A. Karbach, R. Novotny, D. Pelte, and G. Strauch, Nucl. Phys. A **371**, 477 (1981).
[88] D. Pelte, U. Winkler, R. Novotny, and H. Gräf, Nucl. Phys. A **371**, 454 (1981).
[89] C. Manduchi, M. T. Rucco-Manduchi, G. F. Segato, and F. Andolfato Il, Nuovo Cimento **89**, 225 (1985).
[90] Z. Majka, M. E. Brandan, D. Fabris, K. Hagel, A. Menchaca-Rocha, J. B. Natowitz, G. Nebbia, G. Prete, B. Sterling, and G. Viesti, Phys. Rev. C **35**, 2125 (1987).
[91] G. Viesti, B. Fornal, D. Fabris, K. Hagel, J. B. Natowitz, G. Nebbia, G. Prete, and F. Trotti, Phys. Rev. C **38**, 2640 (1988).
[92] B. Fornal *et al.*, Phys. Rev. C **41**, 127 (1990).